PHYSICAL REVIEW D **85,** 075007 (2012)

Focus point supersymmetry redux

Jonathan L. Feng,[1] Konstantin T. Matchev,[2] and David Sanford[3]

[1]*Department of Physics and Astronomy, University of California, Irvine, California 92697, USA*
[2]*Department of Physics, University of Florida, Gainesville, Florida 32611, USA*
[3]*Department of Physics and Astronomy, University of California, Irvine, California 92697, USA*

(Received 27 December 2011; published 5 April 2012)

Recent results from Higgs boson and supersymmetry searches at the Large Hadron Collider provide strong new motivations for supersymmetric theories with heavy superpartners. We reconsider focus point supersymmetry (FP SUSY), in which all squarks and sleptons may have multi-TeV masses without introducing fine-tuning in the weak scale with respect to variations in the fundamental SUSY-breaking parameters. We examine both FP SUSY and its familiar special case, the FP region of minimal supergravity, also known as the constrained minimal supersymmetric standard model (mSUGRA/CMSSM), and show that they are beautifully consistent with all particle, astroparticle, and cosmological data, including Higgs boson mass limits, null results from SUSY searches, electric dipole moments, $b \to s\gamma$, $B_s \to \mu^+\mu^-$, the thermal relic density of neutralinos, and dark matter searches. The observed deviation of the muon's anomalous magnetic moment from its standard model value may also be explained in FP SUSY, although not in the FP region of mSUGRA/CMSSM. In light of recent data, we advocate refined searches for FP SUSY and related scenarios with heavy squarks and sleptons, and we present a simplified parameter space within mSUGRA/CMSSM to aid such analyses.

DOI: 10.1103/PhysRevD.85.075007 PACS numbers: 12.60.Jv, 11.30.Pb, 95.35.+d

I. INTRODUCTION

Since its discovery decades ago, supersymmetry (SUSY) has attracted more attention than any other principle for physics beyond the standard model (SM). Of particular interest is weak-scale SUSY, which holds the promise of providing natural resolutions to the gauge hierarchy and dark matter problems. For the last year, the Large Hadron Collier has been colliding protons with protons at a center-of-mass energy of 7 TeV. The ATLAS and CMS experiments have each analyzed over 1 fb^{-1} of data and collected over 5 fb^{-1}, but have not reported evidence for new physics [1–6]. These null results have excluded generic SUSY models with light superpartners and large missing E_T signatures.

Although these LHC results have disappointed the most optimistic SUSY enthusiasts, they do not remove the possibility that weak-scale SUSY is realized in nature. Rather, they shift attention to supersymmetric models that have heavier superpartners or less distinctive signatures. The former possibility is particularly natural to consider, since stringent constraints on flavor and *CP* violation have long motivated heavy squarks and sleptons of the first two generations, and experimental bounds on the Higgs boson mass have long motivated heavy third generation squarks to raise the Higgs boson mass through large radiative corrections. This possibility has now received even greater motivation from recent results from the ATLAS and CMS experiments, which combined confine the possibility of a light Higgs boson to the mass window $115.5\ \text{GeV} < m_h < 127\ \text{GeV}$, and indicate excess events consistent with the production of Higgs bosons with masses of 126 GeV and 124 GeV, respectively [7,8]. Of course, the possibility of multi-TeV third generation squarks is generically in tension with the requirement that SUSY resolve the gauge hierarchy problem.

In this study, we consider focus point (FP) SUSY [9–12] in light of recent results. We are motivated to consider FP SUSY for several reasons. First, in FP SUSY, *all* squarks and sleptons may be multi-TeV without increasing the fine-tuning in the weak scale with respect to variations in the fundamental SUSY-breaking parameters. Naturalness is a notoriously brittle and subjective criterion, but in this sense, FP SUSY is the unique framework that naturally accommodates multi-TeV top and bottom squarks. Second, many observables, including those at colliders, in low-energy probes, and those related to dark matter, are insensitive to the details of the heavy scalar spectrum, since the scalars decouple. For these observables, FP SUSY may be viewed as an effective theory that captures the essential features of a large class of models with heavy superpartners. And last, a special case of FP SUSY is realized in the FP region of minimal supergravity (mSUGRA) or the constrained minimal supersymmetric standard model (CMSSM), heretofore referred to as the "FP region." Given the amount of work devoted to this model, FP SUSY is a practical and natural starting place for considering SUSY models with heavy superpartners that are newly motivated by LHC data. For other recent work on FP SUSY and the related framework of hyperbolic branch SUSY [13] motivated by recent results, see Refs. [14,15].

We begin in Sec. II by reviewing the general framework of FP SUSY and its well-known special case, the FP region.

In Sec. III, we show Higgs mass predictions in mSUGRA/CMSSM, determine the parameter space favored by Higgs mass bounds, and find that current limits favor the FP region. In Sec. IV we show that constraints on the electron and neutron electric dipole moments (EDMs) are naturally satisfied in FP SUSY. In Sec. V, we then focus on the part of the FP region that has the correct neutralino thermal relic density Ω_χ. This is typically presented as a thin strip in the $(m_0, M_{1/2})$ plane with fixed $\tan\beta$. To allow a more comprehensive presentation of FP results, we instead fix m_0 to give the correct Ω_χ, and present results in the $(\tan\beta, M_{1/2})$ plane, with every point satisfying $\Omega_\chi \simeq 0.23$. In Sec. VI we present results for $b \to s\gamma$ and $B_s \to \mu^+\mu^-$ in the $(\tan\beta, M_{1/2})$ plane, and in Sec. VII we analyze implications for dark matter direct detection and show that FP SUSY remains consistent with current null results. Finally, in Sec. VIII we show that the observed deviations of $(g-2)_\mu$ from SM expectations may be easily explained in FP SUSY (but not in the FP region). Our findings are summarized in Sec. IX. The robustness of our numerical analyses is discussed in the Appendix.

II. FOCUS POINT SUPERSYMMETRY

In SUSY, the Z boson mass is determined at tree level by the relation

$$\frac{1}{2}m_Z^2 = -\mu^2 + \frac{m_{H_d}^2 - m_{H_u}^2\tan^2\beta}{\tan^2\beta - 1}\Bigg|_{m_{\rm weak}}, \tag{1}$$

where μ is the Higgsino mass parameter, $m_{H_{d,u}}^2$ are the soft SUSY-breaking Higgs mass parameters, $\tan\beta \equiv \langle H_u^0\rangle/\langle H_d^0\rangle$ is the ratio of Higgs boson vacuum expectation values, and all of these are evaluated at a renormalization-group scale near $m_{\rm weak} \sim 100$ GeV $-$ 1 TeV. For the moderate and large values of $\tan\beta$ required by current Higgs mass bounds, this may be simplified to

$$\tfrac{1}{2}m_Z^2 \approx -\mu^2 - m_{H_u}^2|_{m_{\rm weak}}. \tag{2}$$

The weak-scale parameter $m_{H_u}^2$ depends on a set of fundamental parameters $\{a_i\}$, typically taken to be grand unified theory (GUT)-scale soft SUSY-breaking parameters, such as scalar masses $m_{\tilde f}$, gaugino masses M_i, and trilinear scalar couplings A_i. Naturalness requires that m_Z not be unusually sensitive to variations in the fundamental parameters a_i. This does not necessarily imply $a_i \sim m_Z$ for every i, however, because terms involving some a_i in the expression for m_Z^2 may be suppressed by small numerical coefficients.

In the class of FP SUSY models studied in Refs. [9–12], the fundamental GUT-scale parameters satisfy

$$(m_{H_u}^2, m_{T_R}^2, m_{(T,B)_L}^2) = m_0^2(1, 1+x, 1-x), \tag{3}$$

$$\text{all other scalar masses} \lesssim \mathcal{O}(10\ \text{TeV}), \tag{4}$$

$$M_i, A_i \lesssim 1\ \text{TeV}, \tag{5}$$

for moderate $\tan\beta$, or

$$(m_{H_u}^2, m_{T_R}^2, m_{(T,B)_L}^2, m_{B_R}^2, m_{H_d}^2) = m_0^2(1, 1+x, 1-x, 1+x-x', 1+x'), \tag{6}$$

$$\text{all other scalar masses} \lesssim \mathcal{O}(10\ \text{TeV}), \tag{7}$$

$$M_i, A_i \lesssim 1\ \text{TeV}, \tag{8}$$

for high $\tan\beta$, where the top and bottom Yukawa couplings are comparable. In Eqs. (3) and (6), x and x' are arbitrary constants, but for any values of x and x', the weak scale is insensitive to variations in m_0, even for multi-TeV m_0. In other words, with these GUT-scale boundary conditions, renormalization-group evolution takes $m_{H_u}^2$ to values around m_Z^2 at the weak scale, almost independent of its initial GUT-scale value. This ''focusing'' of renormalization-group trajectories does not apply to the top and bottom squark masses or, of course, to any other squark and slepton masses. As a result, in FP SUSY, all squarks and sleptons may have multi-TeV masses without introducing fine-tuning in the electroweak scale with respect to variations in the fundamental soft SUSY-breaking parameters. For an extended discussion of naturalness in FP SUSY, see Ref. [11].

As evident from Eqs. (3) and (6), the framework of FP SUSY is quite general. If one assumes that $x = x' = 0$, that all other sfermion masses are also unified to the same m_0, that all gaugino masses are unified, and that all A-parameters are unified, FP SUSY parameter space intersects the mSUGRA/CMSSM parameter space in what is known as the FP region. In general, however, FP SUSY requires neither gaugino mass nor A-parameter unification, and also does not constrain scalar masses that are only weakly coupled to the Higgs sector, such as the first and second generation squark and slepton masses. In much of the analysis below, we will consider the FP region, as in many cases, it serves as an adequate representative of general FP SUSY. The distinction between FP SUSY and the FP region will be relevant, however, when we discuss FP SUSY predictions for $(g-2)_\mu$ in Sec. VIII.

III. HIGGS BOSON MASS

As is well known, current bounds from LEP2 require the Higgs boson mass to be $m_h > 114.4$ GeV [16]. In SUSY, where the limit $m_h \le m_Z$ applies at tree level, large radiative corrections from heavy top and bottom squarks are required to satisfy this bound. A significant phenomenological advantage of the FP SUSY framework is that it naturally accommodates heavy third generation squarks, and with them, relatively heavy Higgs bosons consistent with the LEP2 bound. Given recent Higgs boson results from the LHC [7,8], it is, of course, also interesting to

investigate whether Higgs boson masses in the allowed window $115.5\ \text{GeV} < m_h < 127\ \text{GeV}$ are possible, and whether masses as large as $\sim$125 GeV may be naturally accommodated.

In Fig. 1, we plot contours of constant Higgs boson mass m_h in the $(m_0, M_{1/2})$ plane of mSUGRA/CMSSM. Also shown is the contour on which the neutralino relic density satisfies $\Omega_\chi \simeq 0.23$. Here and throughout we use SOFTSUSY 3.1.7 [17] to generate the SUSY spectrum, and MICROMEGAS 2.4 [18] to calculate the relic density and several other observables. In each case, we use a top quark mass of $m_t = 173.1$ GeV and strong coupling constant $\alpha_s(M_Z) = 0.1172$.

Restricting attention to the cosmologically favored contour with $\Omega_\chi \simeq 0.23$, we see that the Higgs mass bound $m_h > 114.4$ GeV requires either $m_0 \gtrsim 2$ TeV (the FP region), or very low m_0 and $M_{1/2} \gtrsim 500$ GeV (the coannihilation region). For the parameters plotted, then, the LEP2 Higgs mass bound has already eliminated much of the parameter space now excluded by null results from LHC SUSY searches. In the FP region, the Higgs boson mass satisfies $m_h \gtrsim 114$ GeV, and extends up to 122 GeV (124 GeV) for $M_{1/2} \sim 1$ TeV (2 TeV). Given an estimated 2–3 GeV uncertainty in the Higgs boson mass calculation [17,19,20], the FP region beautifully predicts Higgs boson masses in the currently allowed range from 115.5 GeV to 127 GeV, and also naturally accommodates the 124–126 GeV mass range tentatively indicated by LHC search results. Varying A_0 within the range $|A_0| \lesssim$ TeV can also raise the Higgs boson mass slightly by $\sim$1 GeV.

Contours of constant dark matter mass m_χ are also shown. Note that $m_\chi \sim \mathcal{O}(100\ \text{GeV})$, even for multi-TeV m_0 in the cosmologically favored regions. The viable FP region contains heavy sleptons and squarks, but potentially sub-TeV gluinos, electroweak gauginos and Higgsinos as light as 200 GeV, and neutralino dark matter as light as 100 GeV, even under the restrictive assumption of gaugino mass unification. We will return to the cosmological implications of FP SUSY in Sec. VII.

IV. ELECTRIC DIPOLE MOMENTS

FP SUSY is also motivated by constraints from EDMs. Generic SUSY theories with weak-scale superpartners violate low-energy flavor- and CP-violation constraints. Although there are well-known mechanisms to suppress flavor violation, these do not typically suppress CP violation. In general, all gaugino masses, A-terms, and the μ parameter can possess phases that give rise to CP violation. The most limiting CP-violating, but flavor-conserving, observables are the EDMs of the electron and neutron, which can arise from loop diagrams with either left-right sfermion mixing or a gaugino-Higgsino flip within the loop. Even with $A \neq 0$, left-right mixing for first generation sfermions is typically negligible, but an EDM contribution can still arise if there is a mismatch between the phases of the gaugino masses and the phase of μ.

To examine these effects, we consider a simple extension of mSUGRA/CMSSM where the gaugino masses and μ have general CP-violating phases and the mismatch is parametrized as ϕ_{CP}. The dominant diagrams involve

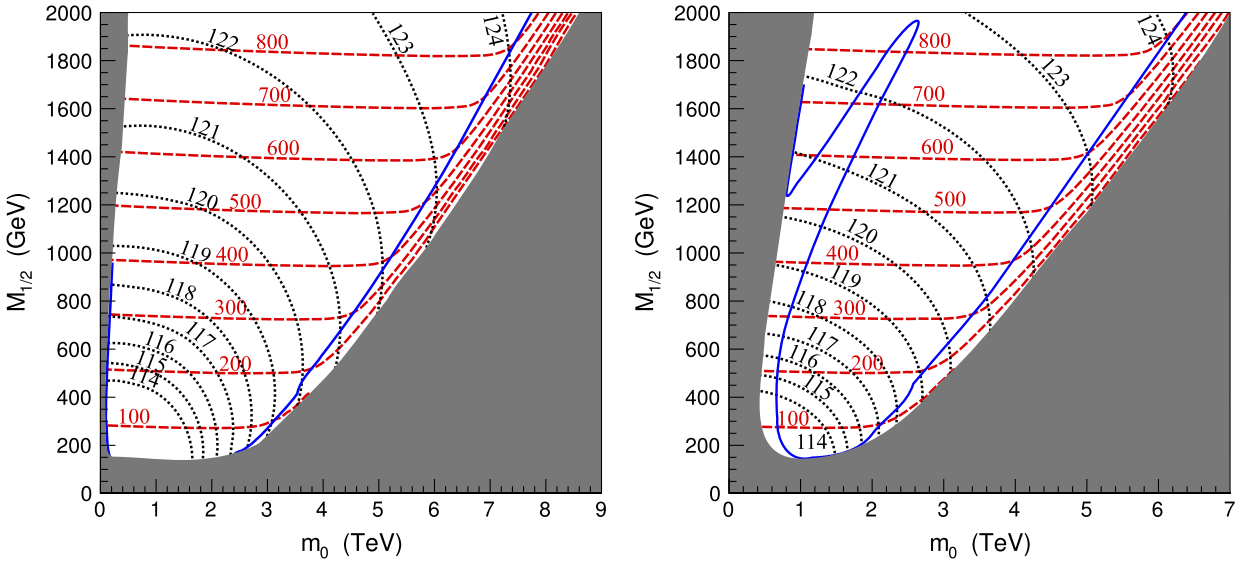

(a) m_h and m_χ in GeV for $\tan\beta = 10$ (b) m_h and m_χ in GeV for $\tan\beta = 50$

FIG. 1 (color online). Contours of the light Higgs boson mass m_h in black (dotted) and lightest neutralino mass m_χ in red (dashed) in the $(m_0, M_{1/2})$ plane for $\tan\beta = 10$ (a) and 50 (b), $A_0 = 0$, and $\mu > 0$. On the blue (solid) lines, the neutralino relic density is $\Omega_\chi \simeq 0.23$.

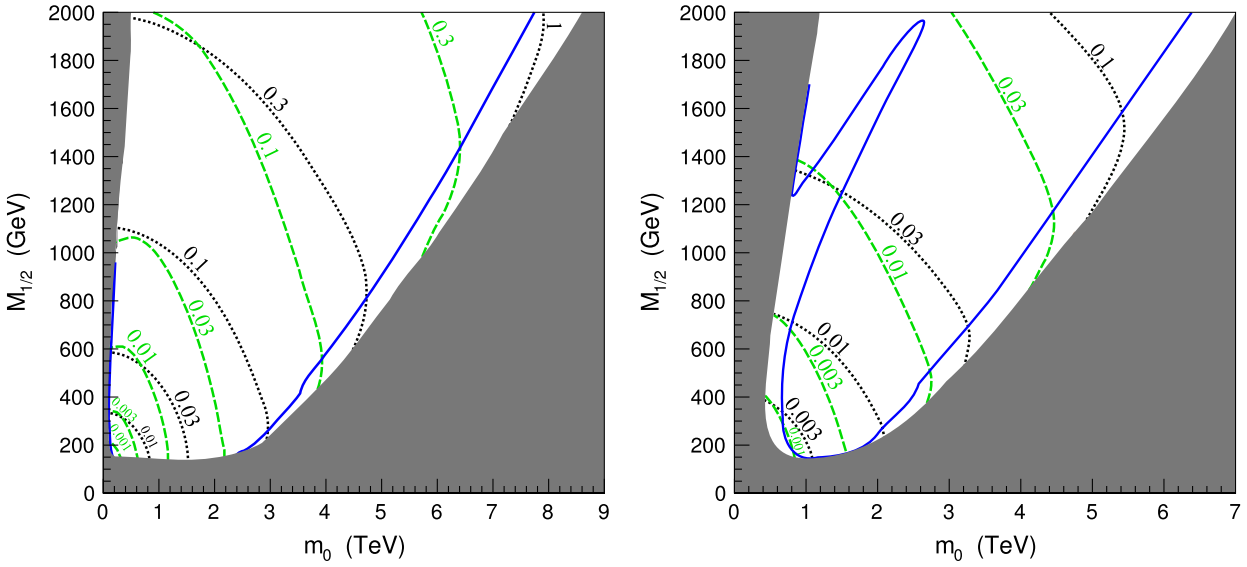

(a) Upper limits on $\sin\phi_{\rm CP}$ for $\tan\beta = 10$ (b) Upper limits on $\sin\phi_{\rm CP}$ for $\tan\beta = 50$

FIG. 2 (color online). Upper limits on $\sin\phi_{CP}$ from neutron EDM constraints in black (dotted) and electron EDM constraints in green (dashed) for $\tan\beta = 10$ (a) and 50 (b), $A = 0$, and $\mu > 0$. On the blue (solid) line, the neutralino relic density is $\Omega_\chi \simeq 0.23$.

left-handed sfermions and charginos with a wino-Higgsino mixture, leading to contributions [21]

$$d_f = \tfrac{1}{2} e m_f g_2^2 |M_2 \mu| \tan\beta \sin\phi_{CP} K_C(m^2_{\tilde{f}_L}, |\mu|^2, |M_2|^2), \quad (9)$$

where K_C is a kinematic function [22]. Diagrams involving sfermions and neutralinos produce subdominant contributions.

The current bounds on the electron and neutron EDMs are $d_e < 1.6 \times 10^{-27} e\,\text{cm}$ [23] and $d_n < 2.9 \times 10^{-26} e\,\text{cm}$ [24]. Assuming $m_u = 3$ MeV, $m_d = 5$ MeV, the naive quark model relation $d_n = (4d_d - d_u)/3$, and neglecting cancellations between different diagrams, we may derive bounds on the phase mismatch ϕ_{CP}.

Figure 2 shows the upper limits on $\sin\phi_{CP}$ in the $(m_0, M_{1/2})$ plane from electron and neutron EDM constraints. In mSUGRA, $m_{\tilde{e}_L} < m_{\tilde{u}_L} \simeq m_{\tilde{d}_L}$, and so the electron EDM provides the stronger bound, but the neutron EDM bound is also stringent. From Fig. 2(a), for example, we see that for $\tan\beta = 10$, the constraints $\Omega_\chi \simeq 0.23$ and $\sin\phi_{CP} \gtrsim 0.01$ can only be satisfied in the FP region, and at the same time, the FP region with $M_{1/2} \lesssim 1$ TeV can accommodate natural values of $\sin\phi_{CP} \sim 0.3$. The EDM bounds become even stronger for large $\tan\beta$, but may be satisfied in the FP region for $M_{1/2} \sim 2$ TeV for $\sin\phi_{CP} \sim 0.1$. Absent a compelling mechanism for suppressing flavor-conserving CP violation, bounds from electron and neutron EDMs have long ago restricted mSUGRA/CMSSM parameter space to the FP region, irrespective of recent LHC results from SUSY and Higgs boson searches.

V. FP SUSY WITH FIXED RELIC DENSITY

Results for the mSUGRA/CMSSM framework are conventionally presented as in Figs. 1 and 2. In these figures, the cosmologically desirable region with $\Omega_\chi \simeq 0.23$ is just a thin strip running through the plane, and the cosmologically desirable FP region is just a small part of that. However, given that much of the rest of the cosmologically favored mSUGRA parameter space is now excluded, in addition to studying FP SUSY in general, it is appropriate to consider a parameter space in which every point is in the cosmologically favored part of the FP region.

For a neutralino lightest supersymmetric particle (LSP) in the FP region, a significant bino-Higgsino mixture is required to produce a sufficiently low relic density, with the Higgsino component increasing with m_0. Thus the value of m_0 satisfying $\Omega_\chi \simeq 0.23$ for a particular set of other parameters represents a lower bound. If the neutralino composes only a fraction of the relic density, $\Omega_\chi < 0.23$, scalar masses are increased somewhat and the primary effect on our conclusion is a weakening of direct detection limits. It is also possible to disconnect the FP effect on fine-tuning from cosmological considerations by introducing a gravitino LSP which allows a larger neutralino relic density to be considered; we restrict our intention to the case of a neutralino LSP.

To satisfy the relic density constraint, we continue to consider fixed values of A_0 and $\text{sgn}(\mu)$, but require the neutralino to be a thermal relic with $\Omega_\chi = 0.23$. This implies a constraint on the remaining parameters m_0,

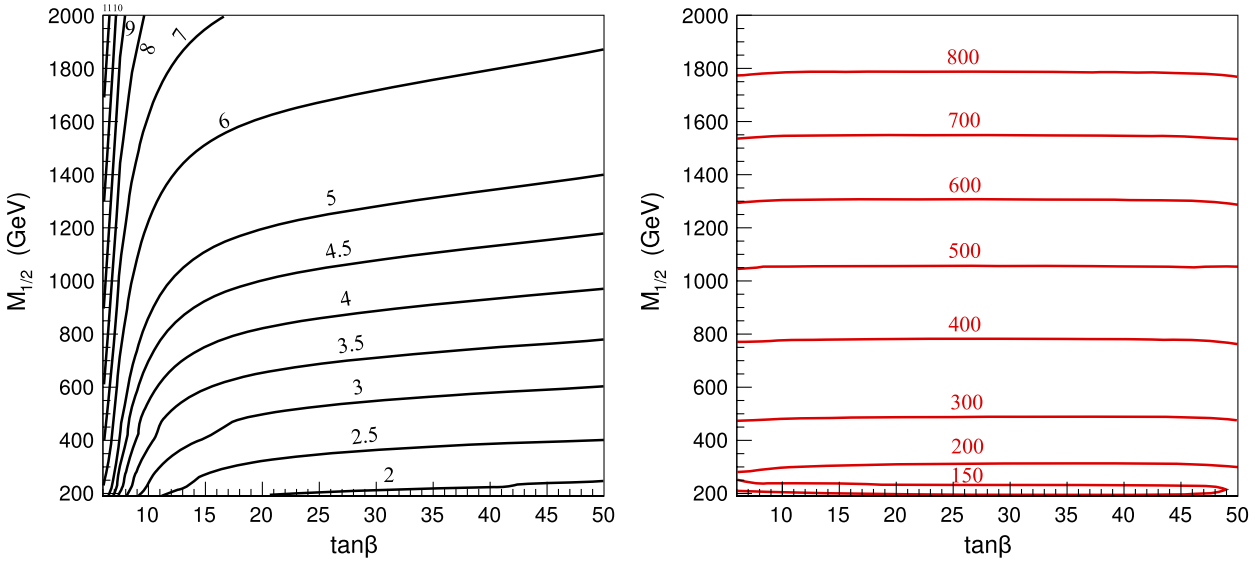

(a) m_0 (TeV) (b) μ (GeV)

FIG. 3 (color online). Contours of (a) m_0 (in TeV) and (b) μ (in GeV) in the $(\tan\beta, M_{1/2})$ plane. Every point in the parameter space is in the FP region and satisfies $\Omega_\chi \simeq 0.23$, $A_0 = 0$, and $\mu > 0$.

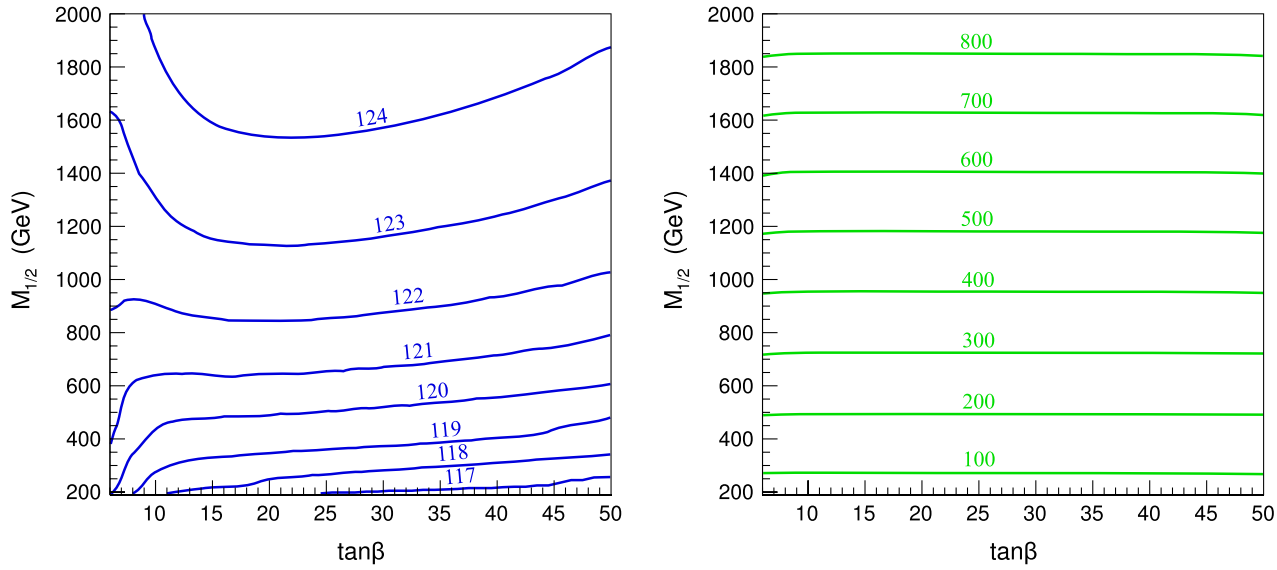

(a) m_h (GeV) (b) m_χ (GeV)

FIG. 4 (color online). Contours of m_h (a) and m_χ (b) in the $(\tan\beta, M_{1/2})$ plane. Every point in the parameter space is in the FP region and satisfies $\Omega_\chi \simeq 0.23$, $A_0 = 0$, and $\mu > 0$.

$M_{1/2}$, and $\tan\beta$. We choose $M_{1/2}$ and $\tan\beta$ as the free parameters, and use Ω_χ to determine m_0.[1] In general there are several values of m_0 satisfying this condition for a particular $(M_{1/2}, \tan\beta)$ pair, arising from the coannihilation region at low m_0, the FP region at large m_0, and the A-funnel region for moderate m_0 and large $\tan\beta$. We focus on the FP region by always choosing the largest value of m_0 for a given point in the $(M_{1/2}, \tan\beta)$ plane.

In Fig. 3, we show contours of constant m_0 and μ in the $(\tan\beta, M_{1/2})$ parameter space defined above, where every point has $\Omega_\chi \simeq 0.23$, $A_0 = 0$, and $\mu > 0$. In Fig. 3(a), we see that m_0 increases as $M_{1/2}$ increases and decreases as $\tan\beta$ increases. In the FP region, the large mass of the

[1]Alternatively, one could choose $M_{1/2}$ and m_0 as the input parameters, and predict $\tan\beta$ [25].

sfermions makes them nearly decoupled for the relic density calculation. The correct value of m_0 is instead solely determined by its impact on the Higgs potential, which sets $|\mu|$, and which in turn determines the correct bino-Higgsino mixture to produce $\Omega_\chi = 0.23$.[2] In Fig. 3(b), we see that μ grows with increasing $M_{1/2}$, but is nearly independent of $\tan\beta$, given the subdominance of terms involving $\tan\beta$ in the neutralino mass matrix.

In Fig. 4, we plot contours of m_h and m_χ in the same $(\tan\beta, M_{1/2})$ parameter space. The large value of $m_{\tilde{t}}$ in the FP region raises the Higgs mass well above the LEP2 bound of 114.4 GeV, and is confined to the currently allowed range of 115.5 GeV $< m_h <$ 127 GeV. As one moves to smaller values of $\tan\beta$, m_h increases even though its tree-level value drops, because of the enhancement of the loop-level contribution from increasing m_0. The neutralino mass contours satisfy $m_\chi \approx M_1 \simeq 0.4 M_{1/2}$, since the neutralino is primarily bino-like, although there is an increasingly significant Higgsino component as $M_{1/2}$ increases. As with the M_1 and μ contours, the m_χ contours are also nearly independent of $\tan\beta$.

VI. RARE B PROCESSES

Rare decays are often used to constrain new physics scenarios, and, in particular, the decays $\bar{B} \to X_s\gamma$ and $B_s \to \mu^+\mu^-$ are well-known probes of new physics. The measured value of $B(\bar{B} \to X_s\gamma)$ is $(3.55 \pm 0.33) \times 10^{-4}$ [28], consistent with the SM value of $(3.15 \pm 0.23) \times 10^{-4}$ [29,30]. The value of $B(B_s \to \mu^+\mu^-)$ has been the subject of recent interest, with a CDF analysis reporting a value of $1.8^{+1.1}_{-0.9} \times 10^{-8}$, and claiming $4.6 \times 10^{-9} < B(B_s \to \mu^+\mu^-) < 3.9 \times 10^{-8}$ at 90% C.L. [31,32]. Meanwhile, CMS and LHCb analyses produced only upper limits at 90% C.L. of 1.9×10^{-8} [33] and 5.6×10^{-8} [34], respectively, and 1.08×10^{-8} [35] from a combined analysis using 2010 LHCb data [36]. The SM value is $(3.19 \pm 0.19) \times 10^{-9}$ [37,38], consistent with the LHC bounds and marginally inconsistent with the CDF analysis.

Figure 5 shows the contributions to $\bar{B} \to X_s\gamma$ and $B_s \to \mu^+\mu^-$ from supersymmetric particles. For both observables, the primary supersymmetric contributions arise from loop diagrams involving either charginos or charged Higgs bosons. For $\bar{B} \to X_s\gamma$, the former produces a suppression in the decay for $\mu > 0$ and an enhancement for $\mu < 0$ and the latter an enhancement for either sign of μ. For $B_s \to \mu^+\mu^-$, the chargino contribution is negative and the charged Higgs contribution positive for either sign of μ. Within the FP region, the chargino diagram dominates. For $\bar{B} \to X_s\gamma$, this puts the supersymmetric result in greater tension with experiment than the SM result for $\mu > 0$, though only significantly so at low $M_{1/2}$ and large $\tan\beta$—the 2σ discrepancy line is plotted in Fig. 5(a). For $\mu < 0$, the contribution is positive and within 2σ of the observed result for the entire $(M_{1/2}, \tan\beta)$ plane. For $B_s \to \mu^+\mu^-$, the supersymmetric contribution in the FP region does not significantly alter the SM prediction, at least relative to current experimental uncertainties.

VII. DIRECT DETECTION OF DARK MATTER

In the cosmologically favored region of the FP region, neutralinos make up the dark matter. These regions of parameter space are then constrained by null results from dark matter searches. In particular, null results from direct detection searches that constrain the spin-independent χ-nucleon cross section σ^p have been advanced as significant constraints on FP SUSY [39–41].

In the absence of large left-right mixing, the dominant contributions to both neutralino annihilation and spin-independent scattering are dependent on the "Higgsino-ness" of the lightest neutralino, defined as

$$a_{\tilde{H}} \equiv \sqrt{|a_{\tilde{H}_u}|^2 + |a_{\tilde{H}_d}|^2}, \tag{10}$$

where the neutralino eigenstate is

$$\chi = a_{\tilde{B}}\tilde{B} + a_{\tilde{W}}\tilde{W} + a_{\tilde{H}_u}\tilde{H}_u + a_{\tilde{H}_d}\tilde{H}_d. \tag{11}$$

Figure 6(a) shows the dependence of $a_{\tilde{H}}$ on m_χ in the FP region. The Higgsino-ness generically increases with m_χ to offset the suppression in annihilation from the lowered cross section. However, it decreases when new annihilation channels open at $m_\chi \sim m_W$, m_Z, and $m_\chi \sim m_t$. Figure 6(a) also shows curves in which the neutralino makes up only a fraction of the relic density—for lower relic densities, $a_{\tilde{H}}$ increases to enhance the annihilation rate. The curves are generated by varying $M_{1/2}$ up to 1 TeV, for fixed $\tan\beta = 10$, $A_0 = 0$, and $\mu > 0$.

To determine the spin-independent χ-nucleon cross section σ^p, the contributions of the couplings to each individual quark must be considered. The individual couplings must be weighted according to the scalar quark form factors f_q^N, typically parametrized as

$$\langle N|m_q\bar{\psi}_q\psi_q|N\rangle = f_q^N M_N. \tag{12}$$

The parameters $f_{u,d}^N$ are reasonably well known, and the heavy quark contributions are set by loop contributions using the gluon form factor. However, the value of f_s^N is less certain, given discrepancies between current experimental and lattice results, and this is a well-known source of uncertainty for direct detection predictions [40,42,43].

[2]The determination of m_0 in Fig. 3(a) is sensitive to the value of the top mass (see, e.g., Ref. [26]), and varies somewhat for different MSSM spectrum generation programs. The determination of μ shown in Fig. 3(b), however, is preformed directly from a fit to the measured relic density and is thus robust and independent of the value for the top mass or the spectrum generator used [27]. For more details, see the Appendix.

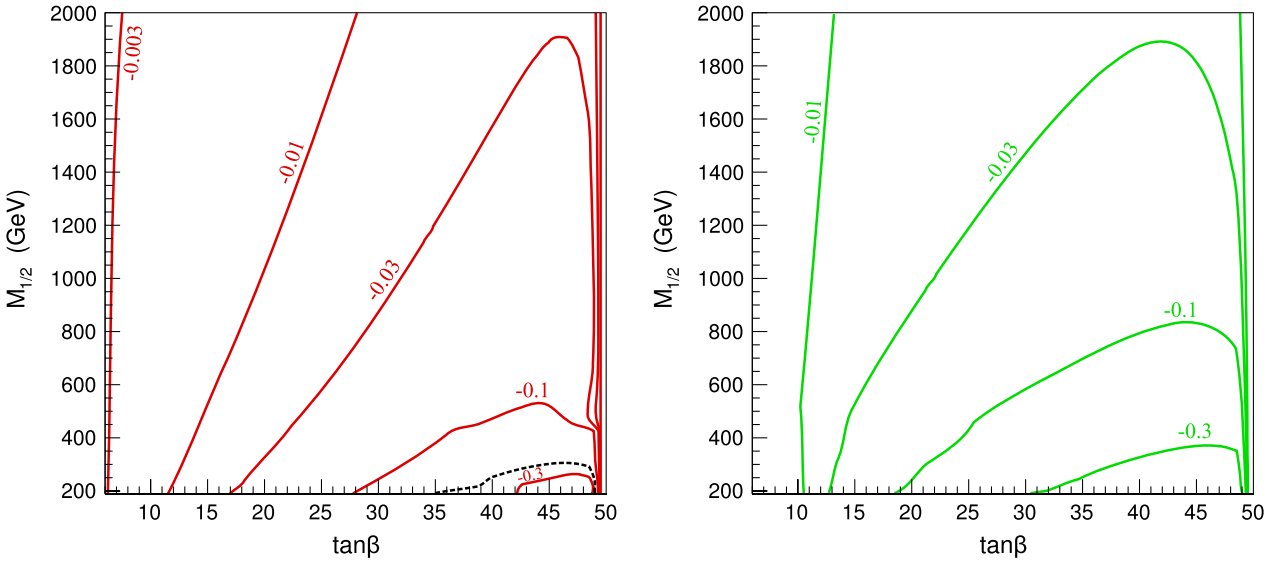

(a) $\Delta B(\bar{B} \to X_s\gamma)$ (b) $\Delta B(B_s \to \mu^+\mu^-)$

FIG. 5 (color online). Contours of $\Delta B(b \to s\gamma)$ in units of 10^{-4} (a) and $\Delta B(B_s \to \mu^+\mu^-)$ in units of 10^{-8} (b) due to SUSY in the $(\tan\beta, M_{1/2})$ plane. Every point in the parameter space is in the FP region and satisfies $\Omega_\chi \simeq 0.23$, $A_0 = 0$, and $\mu > 0$.

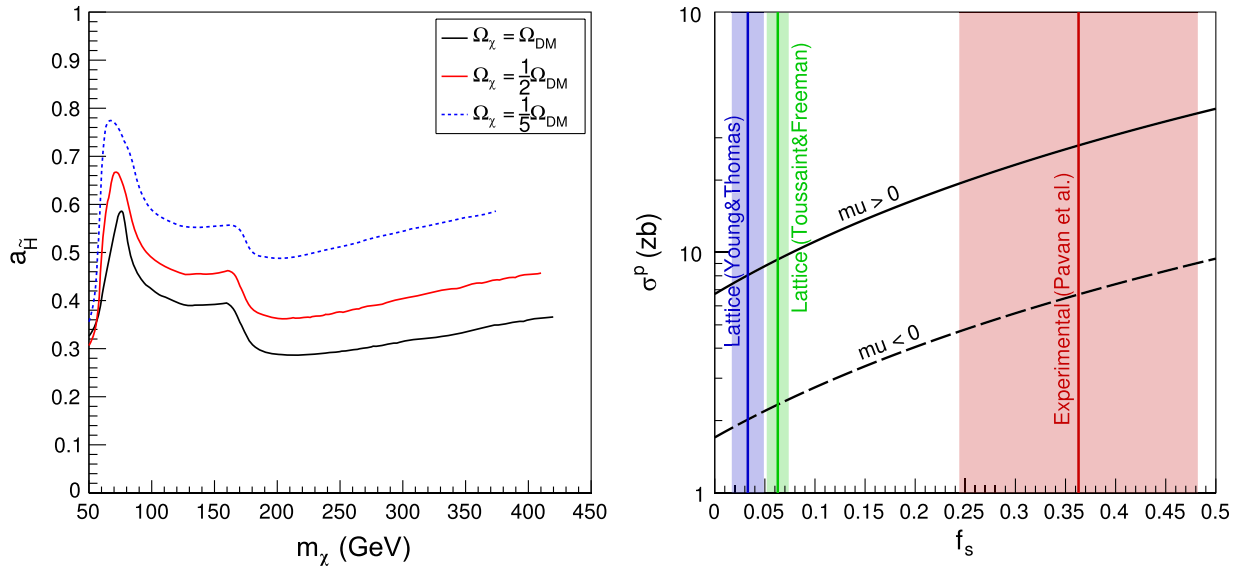

(a) Higgsino content (10) for various relic densities (b) Dependence of σ^p on the strange quark form

FIG. 6 (color online). (a) Higgsino-ness $a_{\tilde{H}}$ for neutralinos in the FP region consistent with various relic densities. The right-most point on each curve corresponds to $M_{1/2} = 1$ TeV. (b) The spin-independent χ-nucleon cross section σ^p as a function of f_s for a model in the FP region with $(m_0, M_{1/2}) = (3\text{ TeV}, 550\text{ GeV})$. The shaded regions indicate the 1σ uncertainties on the various f_s determinations. In both plots, $\tan\beta = 10$, $A_0 = 0$, and $\mu > 0$.

The experimental determination combines a derivation of the pion-nucleon sigma term from meson scattering data [44] combined with a number of chiral perturbation theory results [45–47], giving

$$f_s = f_s^n = f_s^p \sim 0.36. \tag{13}$$

More recent calculations support older determinations of the pion-nucleon sigma term [48]. For this value of f_s, the other form factors are all much smaller, $f^N_{q\neq s} \lesssim 0.05$, and so the strange quark contribution dominates the direct detection cross section [42]. However, two recent lattice studies have found much smaller values for f_s [49,50],

with an average of $f_s \approx 0.05$. For this value of f_s, the strange quark contribution is much closer to that of the other quark flavors [43,51].

Figure 6(b) shows the dependence of σ^p on f_s for both positive and negative μ in the FP region. The value of σ^p varies by a factor of ~ 3 between the experimental and lattice determinations of f_s, which has significant implications for direct detections bounds. The scattering cross section may also be suppressed if $\mu < 0$. This possibility is often ignored in studies that assume $\mu > 0$ to reduce the discrepancy in $(g-2)_\mu$ between the SM and experimental data.

Figure 7 shows contours of σ^p for positive and negative μ and f_s consistent with experimental and lattice results. The general factor of ~ 3 due to different values of f_s is once again apparent. The cross section σ^p for $\mu < 0$ also shows a general suppression relative to that for $\mu > 0$, though the suppression varies significantly with both mass scale and $\tan\beta$. For $\mu > 0$, there is a general enhancement in σ^p at low $\tan\beta$ due to the coupling to the light Higgs, and at high $\tan\beta$ due to a reduction in the masses of the heavy Higgs bosons. These effects are also present for $\mu < 0$, but instead produce a suppression.

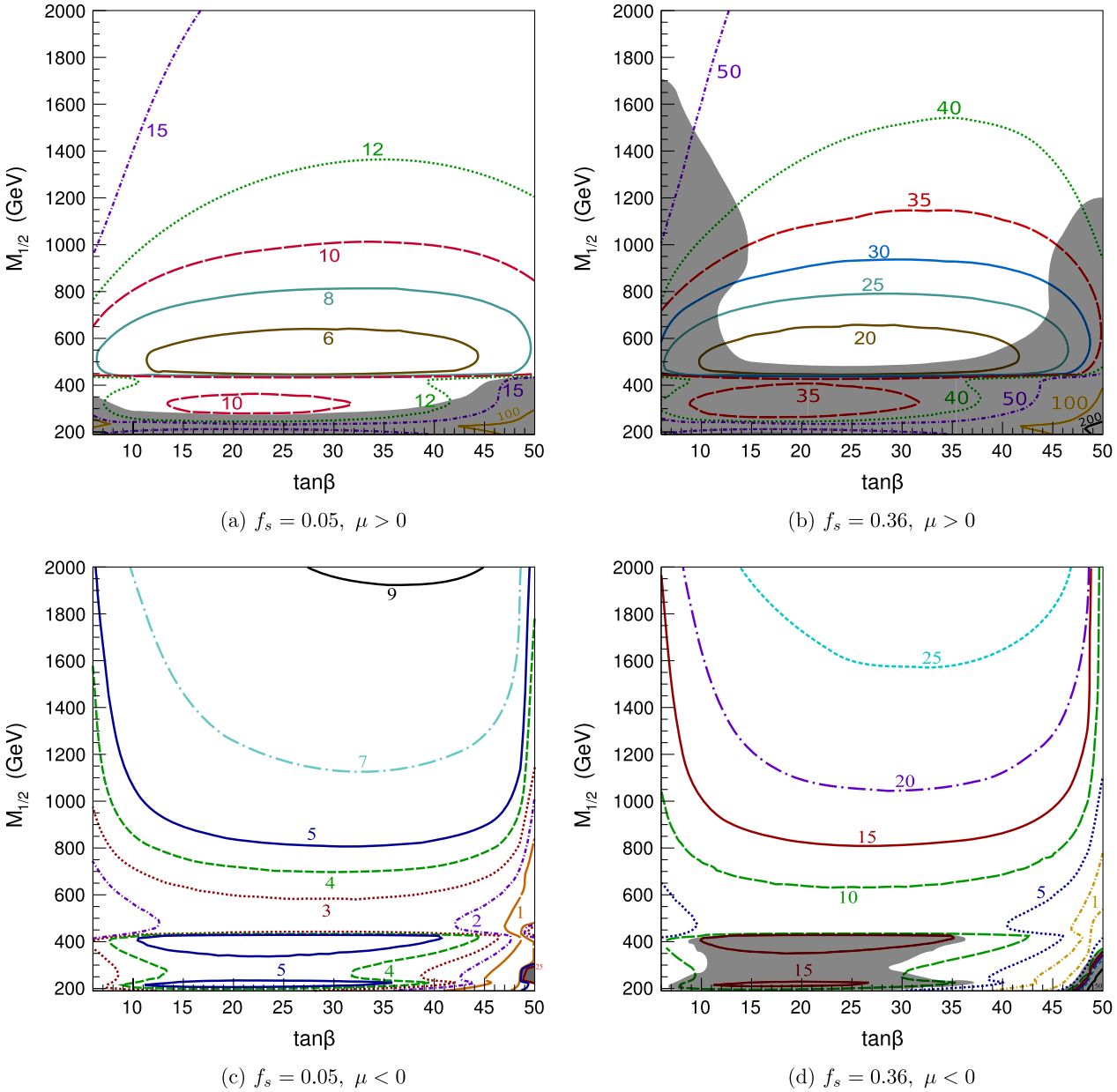

(a) $f_s = 0.05,\ \mu > 0$

(b) $f_s = 0.36,\ \mu > 0$

(c) $f_s = 0.05,\ \mu < 0$

(d) $f_s = 0.36,\ \mu < 0$

FIG. 7 (color online). Contours of σ^p in zeptobarns for $\mu > 0$ (top panels) and for $\mu < 0$ (bottom panels), with $f_s = 0.05$ (left panels) and $f_s = 0.36$ (right panels). In each panel, the shaded region is excluded by XENON100 [52].

Figure 7 also shows the regions of parameter space excluded by XENON100 [52]. For $\mu > 0$, $f_s = 0.05$ in Fig. 7(a), $M_{1/2} < 300$ GeV is excluded for all tanβ, with stronger exclusion at low and high tanβ. The case of $f_s = 0.36$ in Fig. 7(b) is markedly different, with exclusion up to $M_{1/2} \approx 500$ GeV for all tanβ and larger $M_{1/2}$ for low and high tanβ. The same trend carries over to $\mu < 0$—in Fig. 7(c) the exclusion is limited to a small region at high tanβ where scattering is dominated by the heavy-Higgs boson mediated process. The exclusion in Fig. 7(d) is greater due to larger f_s but still reduced compared to the $\mu > 0$ case.

In summary, we find that FP SUSY is far from excluded by current direct detection bounds. For large f_s and $\mu > 0$, significant portions of the parameter space are excluded, but even for these parameters, regions with $M_{1/2} \gtrsim 500$ GeV survive, and for smaller f_s or $\mu < 0$, much of the parameter space is viable. At the same time, it is, of course, interesting that the direct detection bounds are within factors of a few from probing all of FP SUSY. To the extent that LHC SUSY and Higgs boson results motivate SUSY with heavy squarks and sleptons, they also motivate direct detection experiments that are approaching sensitivities to zeptobarn spin-independent cross sections in the near future.

VIII. THE ANOMALOUS MAGNETIC MOMENT OF THE MUON

The well-known $\sim 3\sigma$ discrepancy between the experimental and SM values in the anomalous magnetic moment of the muon [53–55] is currently among the most compelling pieces of evidence for new physics. The supersymmetric contribution is given by $\tilde{\mu} - \chi^0$ and $\tilde{\nu}_\mu - \chi^\pm$ loop diagrams. The $(g-2)_\mu$ discrepancy has two robust implications for SUSY—it is the primary result motivating relatively light superpartners, and it favors $\mu > 0$.

The large sfermion masses in the FP region produce too small a value for $\Delta(g-2)_\mu^{\rm SUSY}$ to explain the observed discrepancy of $(2.9 \pm 0.9) \times 10^{-9}$ [54]. Figure 8 shows the value of $\Delta(g-2)_\mu^{\rm SUSY}$ in the FP region parameter space. The largest value attained is $\Delta(g-2)_\mu^{\rm SUSY} \approx 0.5 \times 10^{-9}$, insufficient to produce even 2σ agreement with the experimental result.

As noted in Sec. II, however, FP SUSY is far more general than the FP region. In particular, in FP SUSY, the smuon and muon sneutrino need not have masses unified with the other scalars, and so may be much lighter than the third generation squarks. To explore this possibility and its implications for $(g-2)_\mu$, we consider the slight modification of mSUGRA/CMSSM in which all scalars have GUT-scale mass m_0, except for the smuons and muon sneutrino. This modification is intended to be schematic, demonstrating the behavior of $(g-2)_\mu$ with lowered smuon masses without bias toward a particular approach.

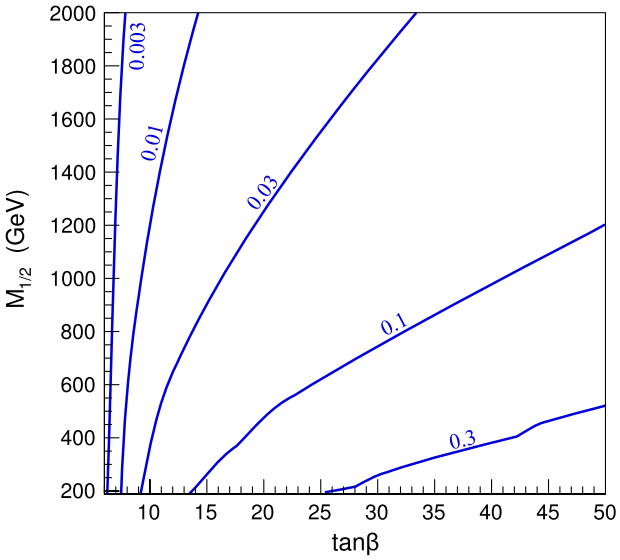

FIG. 8 (color online). Contours of the supersymmetric contribution to $(g-2)_\mu$ in units of 10^{-9}. Every point in the parameter space is in the FP region and satisfies $\Omega_\chi \simeq 0.23$, $A_0 = 0$, and $\mu > 0$.

A fully consistent approach must consider flavor and GUT unification issues. For simplicity, we take the smuon masses to be degenerate at the weak scale, with physical masses

$$M_{\tilde{\mu}} \equiv m_{\tilde{\mu}_L} = m_{\tilde{\mu}_R} = m_{\tilde{\nu}_\mu}. \tag{14}$$

At each point in the $(M_{1/2}, \tan\beta)$ plane, we determine the value of $M_{\tilde{\mu}}$ that gives $\Delta(g-2)_\mu^{\rm SUSY}$ that either brings the theoretical prediction into complete agreement with the central experimental value or reduces the discrepancy to 2σ. Note that the dominant factor in the determination of the relic density is the Higgs soft mass, with the sfermion masses providing subleading effects, as long as $m_{\tilde{q}} \gtrsim 500$ GeV and $m_{\tilde{\ell}} \gtrsim 200$ GeV [56]. The smuons can therefore be quite light without affecting the relic density constraint.

The results are given in Fig. 9. As $M_{1/2}$ increases, the required smuon mass decreases to maintain a constant SUSY contribution to $(g-2)_\mu$, and at some point, the required $M_{\tilde{\mu}}$ becomes too low, as it implies a $\tilde{\mu}$ LSP.[3] The supersymmetric contribution $\Delta(g-2)_\mu^{\rm SUSY}$ also has a linear dependence on tanβ, and so at large tanβ, there are allowed solutions for larger values of $M_{1/2}$ and $M_{\tilde{\mu}}$.

It is important to check that the scenarios for resolving the $(g-2)_\mu$ discrepancy are viable in light of null results from LHC new physics searches. The model-independent bounds on slepton masses are, of course, far weaker than

[3] $M_{\tilde{\mu}}$ is cut off at $1.1 \times m_\chi$ numerically to avoid recalculating the relic density due to $\tilde{\mu} - \chi^0$ coannihilation.

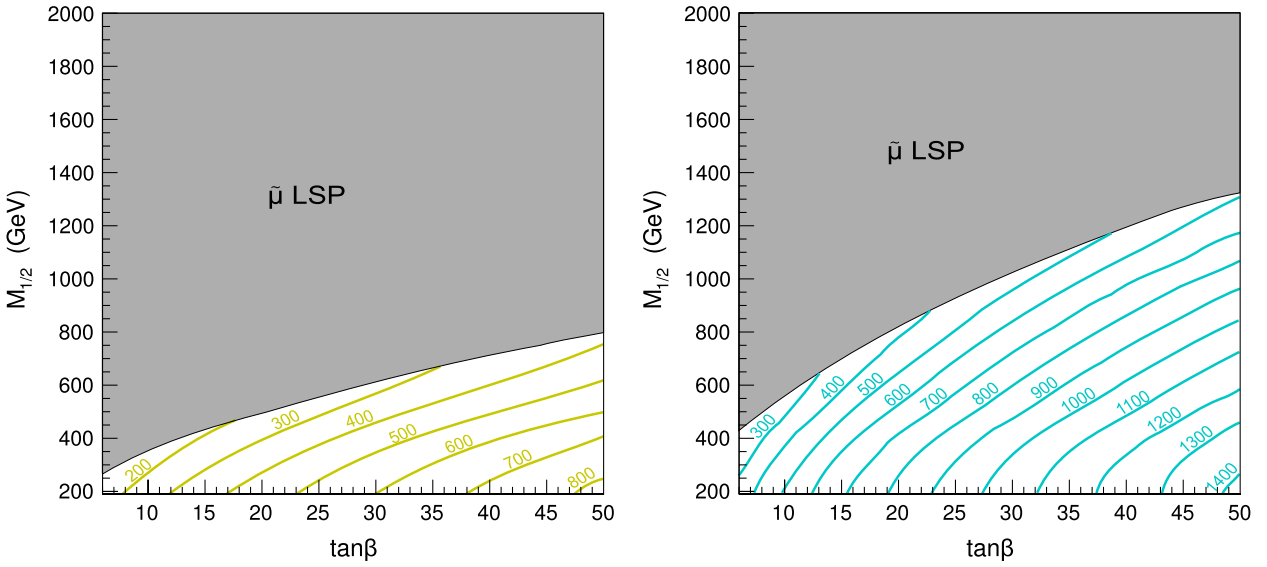

(a) $M_{\tilde{\mu}}$ (GeV) required to eliminate the discrepancy in $(g-2)_\mu$

(b) $M_{\tilde{\mu}}$ (GeV) required to reduce the discrepancy in $(g-2)_\mu$ to 2σ

FIG. 9 (color online). Contours of $M_{\tilde{\mu}}$ required to eliminate the discrepancy between the theoretical and experimental values for $(g-2)_\mu$ (a) and to reduce the discrepancy to 2σ (b). This model framework is a slight modification of mSUGRA/CMSSM in which all scalars have GUT-scale mass m_0, except for the smuons and muon sneutrino, which have physical mass $M_{\tilde{\mu}}$. In the shaded regions, the $\tilde{\mu}$ becomes the LSP. To specify all parameters aside from the smuon and muon sneutrino masses, every point in the parameter space is in the FP region and satisfies $\Omega_\chi \simeq 0.23$, $A_0 = 0$, and $\mu > 0$.

those on squark masses. The best limits on slepton masses are still those from LEP2, which require $m_{\tilde{\mu}} \gtrsim 100$ GeV [57]. In the future, with 30 fb^{-1} of data at 14 TeV, the LHC will be able to discover sleptons through Drell-Yan production for $m_{\tilde{\mu}_L} \lesssim 300$ GeV and $m_{\tilde{\mu}_R} \lesssim 200$ GeV [58]. Greater sensitivity may be available in scenarios where the sleptons are produced in cascades [59]. However, in the FP region where all other scalars are heavy and gluino production dominates, if the sleptons are heavier than all charginos and neutralinos, they will not be produced in gluino cascades, and so the Drell-Yan limits apply. This is the case for regions of the $(\tan\beta, M_{1/2})$ plane shown in Fig. 9, and so there are viable FP SUSY scenarios that resolve the $(g-2)_\mu$ discrepancy. It would, however, be interesting to investigate scenarios motivated by the $(g-2)_\mu$ discrepancy in which sleptons are produced in gluino cascades.

IX. CONCLUSIONS

SUSY models with heavy squarks and sleptons have long been motivated by constraints on flavor and *CP* violation, the LEP2 constraint on the Higgs boson mass, and other constraints, such as proton decay bounds. Recent null results from LHC SUSY searches have further focused attention on this possibility, and the interest in such scenarios is especially heightened by the currently allowed Higgs boson mass window 115.5 GeV $< m_h <$ 127 GeV, and tentative indications from the ATLAS and CMS experiments for a Higgs boson with mass near 125 GeV.

Generic SUSY scenarios with heavy sfermions, and particularly heavy top and bottom squarks, imply fine-tuning of the weak scale, subverting the basic motivation for weak-scale SUSY. In FP SUSY, however, this is not the case. The mass parameter $m_{H_u}^2$ evolves to values around m_Z^2 at the weak scale, almost independent of its GUT-scale starting value. This focusing of renormalization-group trajectories implies that the weak scale in FP SUSY theories is not fine-tuned with respect to variations in the fundamental SUSY-breaking parameters. Note that the evolution of $m_{H_u}^2$ to values around m_Z^2 at the weak scale for a particular choice of GUT-scale parameters is necessary to remove fine-tuning with respect to variations in μ, and is possible for other choices of GUT-scale parameters (see, for example, Ref. [60,61]). However, naturalness with respect to variations in *all* SUSY-breaking parameters requires that $m_{H_u}^2$ evolve to a weak-scale value irrespective of its starting value, and so the focus point behavior of renormalization-group trajectories is an essential feature of any natural theory with multi-TeV top and bottom squarks motivated by the currently allowed Higgs boson mass range.

In this study, we have focused for the most part on models of FP SUSY that are also part of the mSUGRA/CMSSM framework. These FP region models naturally produce Higgs boson masses above the LEP2 bound of 114.4 GeV, and suppress electron and neutron EDMs

sufficiently, even for $\mathcal{O}(1)$ phases. To more globally display the predictions of FP SUSY, we have required $\Omega_\chi \simeq 0.23$ and plotted results in the $(\tan\beta, M_{1/2})$ plane. We find that FP SUSY naturally accommodates Higgs boson masses up to 120-124 GeV, which, given an estimated 2 GeV uncertainty in the theoretical calculation, is consistent with current Higgs boson mass indications. In addition, we have shown that FP SUSY is naturally consistent with constraints from $b \to s\gamma$, $B_s \to \mu^+\mu^-$, and null results from dark matter direct detection experiments. Finally, in general FP SUSY with a nonunified smuon mass, we have found that FP SUSY may resolve the discrepancy in $(g-2)_\mu$ consistent with all current constraints.

Given these successes, it is natural to ask what evidence for FP SUSY should accumulate in the near future if FP SUSY is realized in nature. Certainly the Higgs boson should be discovered with a mass in the currently allowed mass window, and searches for SUSY from gluino pair production, followed by gluinos cascading through charginos and neutralinos are promising for some of the parameter space [62–66]. Equally exciting would be the discovery of dark matter with a spin-independent χ-nucleon cross section near the zeptobarn scale, which is a robust prediction of mixed bino-Higgsino dark matter with heavy squarks and sleptons. Finally, most signals of indirect dark matter detection are also generically enhanced in the FP SUSY scenario [67].

ACKNOWLEDGMENTS

We thank Daniel Feldman and Asesh Krishna Datta for discussions and Wonsang Cho for collaboration in the early stages of this work. The work of J. L. F. and D. S. was supported in part by NSF Grant No. PHY-0970173. The work of K. T. M. was supported in part by DOE Grant No. DE-FG02-97ER41029. The work of D. S. was supported in part by a UC Irvine Graduate Division.

APPENDIX

It is well known that different spectrum calculators do not give identical results for the SUSY mass spectrum, even for the same set of input parameters [68,69]. The reasons for this apparent discrepancy are well understood; see Ref. [27] for a nice summary. Above all, one should keep in mind that the SUSY spectrum is always calculated at a fixed order in perturbation theory, and there is an intrinsic uncertainty due to neglecting the higher-order terms in perturbation theory. The main differences between the various programs arise mostly because they choose to neglect different sets of higher-order terms. For example, one may choose to use either tree-level or one-loop-corrected masses in the radiative corrections, or choose a slightly different value for the matching scale between the SM and the MSSM. In each case, the difference between the two options is a higher-order effect. In this paper, we chose to work with the SOFTSUSY program, but we expect qualitatively similar results from other spectrum generators as well.

On a related topic, each spectrum calculator needs to solve a two-sided boundary value problem, since the boundary conditions for the gauge and Yukawa couplings are specified at the weak scale, while the soft SUSY-breaking parameters are given at the (yet to be determined) GUT scale. The standard approach used by all programs is to apply iterations until converging on a solution. Unfortunately, on occasion one may encounter poor convergence as a sign of a chaotic behavior [70]. This is illustrated in Fig. 10, which takes a slice through the $(m_0, M_{1/2})$ plane of Fig. 2(a) in 5 GeV increments along m_0, for a fixed value of $M_{1/2} = 850$ GeV. Figure 10 shows the chargino mass $M_{\tilde{\chi}_1^+}$ calculated by SOFTSUSY (right axis) and the relic abundance calculated by MICROMEGAS (left axis). We see that at low m_0, SOFTSUSY is able to converge, and both quantities follow a well-defined trend. However, at sufficiently large values of m_0, SOFTSUSY is not able to achieve the desired level of convergence, and the obtained results (upon exiting after a fixed number of iterations) visibly deviate from the expected trend. As seen in Fig. 10, in principle this presents a problem for the correct mapping of the boundary of the region allowed by LEP chargino searches ($M_{\tilde{\chi}_1^+} > 103$ GeV). Fortunately, however, the parameter space points with the desired value of the relic density ($\Omega_\chi h^2 \approx 0.1$) are relatively safe, since they are still well within the region with good convergence, and the maps shown in Figs. 3 and 4 are robust.

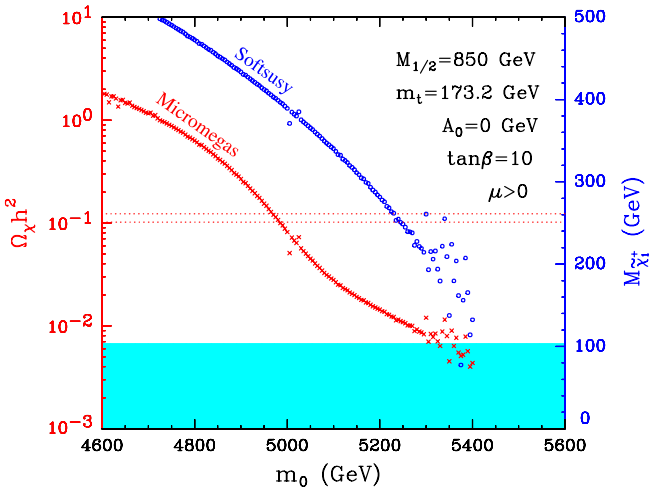

FIG. 10 (color online). A slice through the mSUGRA parameter space from Fig. 2(a) for a fixed $M_{1/2} = 850$ GeV, showing results for the chargino mass $M_{\tilde{\chi}_1^+}$ from SOFTSUSY (blue dots) and for $\Omega_\chi h^2$ from MICROMEGAS (red crosses). The cyan shaded region is excluded by chargino searches at LEP, and the horizontal dotted lines mark the 3σ preferred region for $\Omega_\chi h^2$.

[1] G. Aad *et al.* (ATLAS Collaboration), Phys. Lett. B **710**, 67 (2012).
[2] G. Aad *et al.* (ATLAS Collaboration), J. High Energy Phys. 11 (2011) 099.
[3] G. Aad *et al.* (ATLAS Collaboration), Phys. Rev. D **85**, 012006 (2012).
[4] S. Chatrchyan *et al.* (CMS Collaboration), Phys. Rev. D **85**, 012004 (2012).
[5] S. Chatrchyan *et al.* (CMS Collaboration), Phys. Rev. Lett. **107**, 221804 (2011).
[6] S. Padhi (CMS Collaboration), arXiv:1111.2733.
[7] F. Giannoti (ATLAS Collaboration), ''Update on the Standard Model Higgs Searches in ATLAS,'' https://indico.cern.ch/conferenceDisplay.py?confId=164890.
[8] G. Tonelli (CMS Collaboration), ''Update on the Standard Model Higgs Searches in CMS,'' https://indico.cern.ch/conferenceDisplay.py?confId=164890.
[9] J. L. Feng, K. T. Matchev, and T. Moroi, Phys. Rev. Lett. **84**, 2322 (2000).
[10] J. L. Feng, K. T. Matchev, and T. Moroi, Phys. Rev. D **61**, 075005 (2000).
[11] J. L. Feng and K. T. Matchev, Phys. Rev. D **63**, 095003 (2001).
[12] J. L. Feng, K. T. Matchev, and F. Wilczek, Phys. Lett. B **482**, 388 (2000).
[13] K. L. Chan, U. Chattopadhyay, and P. Nath, Phys. Rev. D **58**, 096004 (1998).
[14] M. Asano, T. Moroi, R. Sato, and T. T. Yanagida, Phys. Lett. B **708**, 107 (2012).
[15] S. Akula, M. Liu, P. Nath, and G. Peim, Phys. Lett. B **709**, 192 (2012).
[16] R. Barate *et al.* (LEP Working Group for Higgs Boson Searches, ALEPH Collaboration, DELPHI Collaboration, L3 Collaboration, and OPAL Collaboration), Phys. Lett. B **565**, 61 (2003).
[17] B. C. Allanach, Comput. Phys. Commun. **143**, 305 (2002).
[18] G. Bélanger, F. Boudjema, P. Brun, A. Pukhov, S. Rosier-Lees, P. Salati, and A. Semenov, Comput. Phys. Commun. **182**, 842 (2011).
[19] G. Degrassi, S. Heinemeyer, W. Hollik, P. Slavich, and G. Weiglein, Eur. Phys. J. C **28**, 133 (2003).
[20] S. Heinemeyer, Int. J. Mod. Phys. A **21**, 2659 (2006).
[21] J. L. Feng, K. T. Matchev, and Y. Shadmi, Nucl. Phys. **B613**, 366 (2001).
[22] T. Moroi, Phys. Rev. D **53**, 6565 (1996).
[23] B. C. Regan, E. D. Commins, C. J. Schmidt, and D. DeMille, Phys. Rev. Lett. **88**, 071805 (2002).
[24] C. A. Baker *et al.*, Phys. Rev. Lett. **97**, 131801 2006).
[25] C. Beskidt, W. de Boer, T. Hanisch, E. Ziebarth, V. Zhukov, and D. I. Kazakov, Phys. Lett. B **695**, 143 (2011).
[26] J. R. Ellis and K. A. Olive, Phys. Lett. B **514**, 114 (2001).
[27] H. Baer, T. Krupovnickas, S. Profumo, and P. Ullio, J. High Energy Phys. 10 (2005) 020.
[28] D. Asner *et al.* (Heavy Flavor Averaging Group), arXiv:1010.1589.
[29] M. Misiak *et al.*, Phys. Rev. Lett. **98**, 022002 (2007).
[30] M. Misiak and M. Steinhauser, Nucl. Phys. **B764**, 62 (2007).
[31] T. Aaltonen *et al.* (CDF Collaboration), Phys. Rev. Lett. **107**, 191801 (2011).
[32] T. Kuhr (CDF Collaboration, arXiv:1111.2428.
[33] S. Chatrchyan *et al.* (CMS Collaboration), Phys. Rev. Lett. **107**, 191802 (2011).
[34] J. Serrano, arXiv:1111.2620.
[35] CMS Collaboration and LHCb Collaboration, ''Search for the Rare Decay $B_s^0 \to \mu^+\mu^-$ at the LHC with the CMS and LHCb Experiments, Combination of LHC Results of the Search for $B_s \to \mu^+\mu^-$ decays,'' http://cdsweb.cern.ch/record/1374913/.
[36] R. Aaij *et al.* (LHCb Collaboration), Phys. Lett. B **699**, 330 (2011).
[37] A. J. Buras, Phys. Lett. B **566**, 115 (2003).
[38] E. Gamiz, C. T. H. Davies, G. P. Lepage, J. Shigemitsu, and M. Wingate (HPQCD Collaboration), Phys. Rev. D **80**, 014503 (2009).
[39] M. Farina, M. Kadastik, D. Pappadopulo, J. Pata, M. Raidal, and A. Strumia, Nucl. Phys. **B853** 607 (2011).
[40] O. Buchmueller, R. Cavanaugh, D. Colling, A. De Roeck, M. Dolan *et al.*, Eur. Phys. J. C **71**, 1722 (2011).
[41] G. Bertone, D. Cerdeno, M. Fornasa, R. de Austri, C. Strege, and R. Trotta, J. Cosmol. Astropart. Phys. 01 (2012) 015.
[42] J. R. Ellis, K. A. Olive, and C. Savage, Phys. Rev. D **77**, 065026 (2008).
[43] J. Giedt, A. W. Thomas, and R. D. Young, Phys. Rev. Lett. **103**, 201802 (2009).
[44] M. M. Pavan, I. I. Strakovsky, R. L. Workman, and R. A. Arndt, PiN Newsletter **16**, 110 (2002).
[45] B. Borasoy and U.-G. Meissner, Ann. Phys. (N.Y.) **254**, 192 (1997).
[46] J. Gasser, H. Leutwyler, and M. E. Sainio, Phys. Lett. B **253**, 260 (1991).
[47] V. Bernard, N. Kaiser, and U.-G. Meissner, Phys. Lett. B **389**, 144 (1996).
[48] J. Alarcon, J. Martin Camalich, and J. Oller, arXiv:1110.3797.
[49] R. D. Young and A. W. Thomas, Phys. Rev. D **81**, 014503 (2010).
[50] W. Freeman and D. Toussaint, Proc. Sci., LAT2009 (2009) 137.
[51] A. W. Thomas, P. E. Shanahan, and R. D. Young, Few-Body Syst. 1 (2012).
[52] E. Aprile *et al.* (XENON100 Collaboration), Phys. Rev. Lett. **107**, 131302 (2011).
[53] G. W. Bennett *et al.* (Muon G-2 Collaboration), Phys. Rev. D **73**, 072003 (2006).
[54] F. Jegerlehner and A. Nyffeler, Phys. Rep. **477**, 1 (2009).
[55] M. Davier, A. Hoecker, B. Malaescu, and Z. Zhang, Eur. Phys. J. C **71**, 1515 (2011).
[56] J. L. Feng and D. Sanford, J. Cosmol. Astropart. Phys. 05 (2011) 018.
[57] J. L. Feng, J.-F. Grivaz, and J. Nachtman, Rev. Mod. Phys. **82**, 699 (2010).
[58] Y. Andreev, S. Bityukov, and N. Krasnikov, Phys. At. Nucl. **68**, 340 (2005).
[59] J. Eckel, W. Shepherd, and S. Su, arXiv:1111.2615.
[60] D. Horton and G. Ross, Nucl. Phys. **B830**, 221 (2010).
[61] D. Feldman, G. Kane, E. Kuflik, and R. Lu, Phys. Lett. B **704**, 56 (2011).
[62] U. Chattopadhyay, A. Datta, A. Datta, A. Datta, and D. Roy, Phys. Lett. B **493**, 127 (2000).

[63] P. Mercadante, J. Mizukoshi, and X. Tata, Phys. Rev. D **72**, 035009 (2005).
[64] U. De Sanctis, T. Lari, S. Montesano, and C. Troncon, Eur. Phys. J. C **52**, 743 (2007).
[65] S. P. Das, A. Datta, M. Guchait, M. Maity, and S. Mukherjee, Eur. Phys. J. C **54**, 645 (2008).
[66] R. Kadala, P. Mercadante, J. Mizukoshi, and X. Tata, Eur. Phys. J. C **56**, 511 (2008).
[67] J. L. Feng, K. T. Matchev, and F. Wilczek, Phys. Rev. D **63**, 045024 (2001).
[68] B. Allanach, S. Kraml, and W. Porod, J. High Energy Phys. 03 (2003) 016.
[69] G. Belanger, S. Kraml, and A. Pukhov, Phys. Rev. D **72**, 015003 (2005).
[70] K. Matchev and R. Remington, arXiv:1202.6580.